

# Prediction of the additional shear action on frame members due to infills

Liborio Cavaleri · Fabio Di Trapani

Received: 10 October 2013 / Accepted: 19 August 2014 / Published online: 2 September 2014  
© Springer Science+Business Media Dordrecht 2014

**Abstract** Infill masonry walls in framed structures make a significant contribution to the response under seismic actions. With special regard to reinforced concrete (RC) structures, it is known that internal forces modifications caused by the frame–infill interaction may be not supported by the surrounding frame because of the additional shear forces arising at the ends of beams and columns. Such additional forces may lead to the activation of brittle collapse mechanisms and hence their prediction is basic in capacity assessment, especially for structures that disregard the details for seismic zones. In this paper a parametric study is carried out addressed to the prediction of the shear forces mentioned before. The results of this study can be used as a support when the simplified model is adopted consisting in the substitution of infill with an equivalent pin jointed concentric strut, because in this case the structural analysis fails in the prediction of the shear forces in question. Through the paper, in which existing RC infilled frames designed only for vertical loads are discussed, analytical laws, depending on the level of the axial force arising in a concentric strut equivalent to infill, are proposed, the above analytical law allowing to correct the local shear forces in the frame critical sections, which are not predictable in the case of substitution of infill with an equivalent concentric strut.

**Keywords** Infilled frames · Masonry infills · Local shear effects · Micromodel · Equivalent strut

## 1 Introduction

The contribution of infills in seismic response of framed reinforced concrete structures is significant; nevertheless, they are usually neglected in models assuming a non-structural function. The seismic damage on this kind of structures suggests, as widely discussed in

---

L. Cavaleri (✉) · F. Di Trapani  
Dipartimento di Ingegneria Civile, Ambientale, Aerospaziale e dei Materiali (DICAM),  
Università degli Studi di Palermo, Viale delle Scienze, 90128 Palermo, Italy  
e-mail: liborio.cavaleri@unipa.it

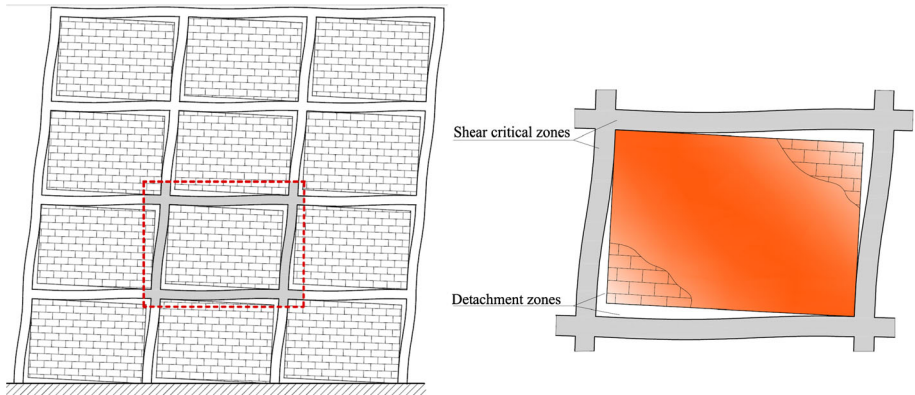


**Fig. 1** Transmission of local shear forces close to the beam–column joints in presence of lateral actions



**Fig. 2** Local shear failure of frame due to interaction with infills under seismic loads

literature, the fact that frames and infills have a strong interaction when involved in seismic events, not always being beneficial for structural safety and not negligible in general.

Though an infilled frame exhibits a significant increase in lateral strength and stiffness with respect to the corresponding bare one this fact cannot be extended to the whole structural behaviour depending on the distribution of infills. It can be generally stated that, if the planar and elevation distributions are regular and approximately symmetric, the contribution of infill panels is beneficial; contrariwise infills are potentially dangerous, often causing activation of additional torsional effects and soft story mechanisms.

Regarding a single frame, the increase in strength mentioned before is associated with an increase in the demand for shear capacity in some specific sections. This aspect of the frame–infill interaction constitutes the central issue of this paper.

As is well known, in the presence of lateral actions, the infill panel partially disconnects from the frame, remaining in contact with it only near two opposite corners (Fig. 1).

Strength increase occurring on infilled frames is allowable, however, if RC members adjacent to panels (beams, columns and joints) have sufficient shear overstrength. When especially strong masonry infill panels are combined with frames having a low shear reinforcement, the activation of local brittle collapse mechanisms, able to compromise the capacity and safety of the entire structure becomes a major question. In Fig. 2 a picture referring to local shear failure mechanism due to frame–infill interaction is reported.

The frame–infill interaction has been treated by several authors which have proposed strategies to introduce the effects of infills in structural models. A very successful technique is based on the replacement of the infill with one or more equivalent diagonal struts. This technique, belonging to the macromodel approaches, was first introduced by Holmes (1961) and then developed by other researchers (Asteris et al. 2011; Chrysostomou and Asteris 2012; Crisafulli et al. 2000).

In the most simple case one equivalent pin-jointed concentric strut is used by means of that it is possible to obtain good reliability in modelling the stiffening effects produced by infill panels (e.g. Papia et al. 2003). Unfortunately, as a counterpart of its simplicity, this approach is unable to provide the internal forces in beams and columns, close to the joints, arising because of frame–infill interaction.

More complex macromodels making use of multiple diagonal struts (two or three), able to reproduce these effects, have also been developed (e.g. Crisafulli and Carr 2007; Fiore et al. 2012). However, identification of the mechanical properties to attribute to each strut is not a simple question since these depend not only on masonry mechanical properties but also on the frame–infill stiffness ratios and on the geometrical characteristics of the system (Asteris 2003, 2008; Cavaleri and Papia 2003). The difficulties in managing multi-strut approaches grow when nonlinear (static or dynamic) analyses are required since the attribution of specific monotonical or cyclic nonlinear laws is necessary for each strut.

A substantially different approach has been instead followed by other authors (e.g. Mallick and Severn 1967; Mehrabi and Shing 1997; Shing and Mehrabi 2002; Ghosh and Made 2002; Asteris 2008; Koutromanos et al. 2011) which have adopted an “exact representation” of infills (micromodelling) to better reproduce frame–infill interaction. According to this modelling approach, panel and frames are modelled by means of planar shell finite elements while interface elements able to reproduce frictional effects and frame–infill detachment are considered for frame–infill contact regions. Such typology of approach, which is aimed at providing a more accurate response, is able to capture well local interaction effects and frame global internal force distribution, but in this case too, calibration of the analytical models, especially in terms of nonlinear laws for shell elements and interfaces, is not easy to accomplish. Furthermore, analyses of framed structures which make use of micromodels require a higher computational effort which is not always acceptable for practical engineering uses.

Also technical codes point out the need to take into account the frame–infill interaction. Eurocode 8 when furnishing indications about modelling in structural analysis prescribes that infill walls which contribute significantly to the lateral stiffness and resistance of building have to be considered. Unfortunately no reference models for infills are provided.

In a similar way in the Italian technical code (D.M. LL. PP. 2008) neither are modelling criteria given nor is a strategy suggested to predict the local increase of shear in the columns and in the beams of infilled frames close to the nodal regions.

Differently from Eurocode 8 and the Italian codes, the Federal Emergency Management Agency code (FEMA 356) dedicates a significant attention to describe how to take infills into account and how to predict the local effects on beams and columns. One possible choice that is offered is to model an infill by an equivalent pin-jointed strut that should have the same thickness and modulus of elasticity as the infill panel while the width  $w$  is given by

$$w = 0.175 (\lambda_1 h')^{-0.4} d \quad (1)$$

where, referring to Fig. 3,  $h'$  is the height of the frame, measured between the centre-lines of the beams,  $d$  is the measure of the diagonal dimension of the infill and  $\lambda_1$  is given by

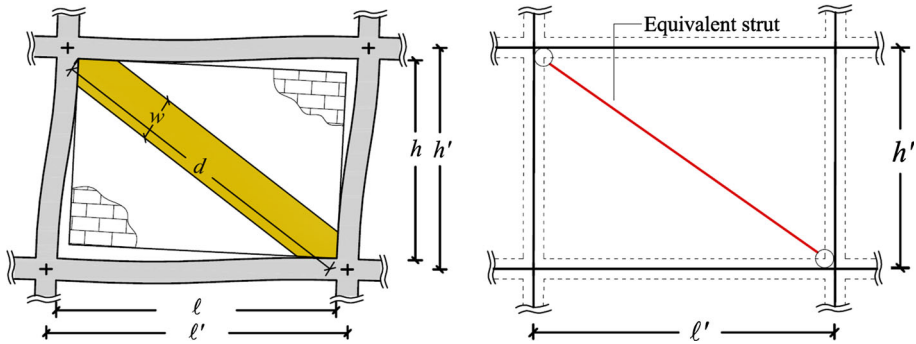


**Fig. 3** Geometrical features of a frame–infill system and of the equivalent diagonal strut

$$\lambda_1 = \left[ \frac{E_d t \sin 2\theta}{4E_f I_c h} \right]^{\frac{1}{4}} \tag{2}$$

in which  $t$  is the thickness of the infill and  $h$  and  $l$  are its height and length, respectively,  $\theta = \text{atan}(h/l)$ ,  $I_c$  is the moment of inertia of the column cross-sections and  $E_d$  and  $E_f$  are the Young’s modulus of the infill and of the material constituting the frame, respectively.

Referring to local interaction effects, the FEMA code specifies that beams and columns adjacent to infills should have sufficient strength to support local shear effects. According to the strategy proposed, in absence of more accurate models and analyses, the FEMA code states that the flexural and shear strength of beams and columns close to nodal regions should exceed the internal forces evaluated by the application, at the specified lengths  $l_{ceff}$  and  $l_{beff}$ , of the horizontal and vertical components of the expected axial force value for an equivalent strut (Fig. 4). The lengths  $l_{ceff}$  and  $l_{beff}$  can be obtained as

$$l_{ceff} = \frac{w}{\cos \theta_c}; \tan \theta_c = \frac{h - l_{ceff}}{l} \tag{3}$$

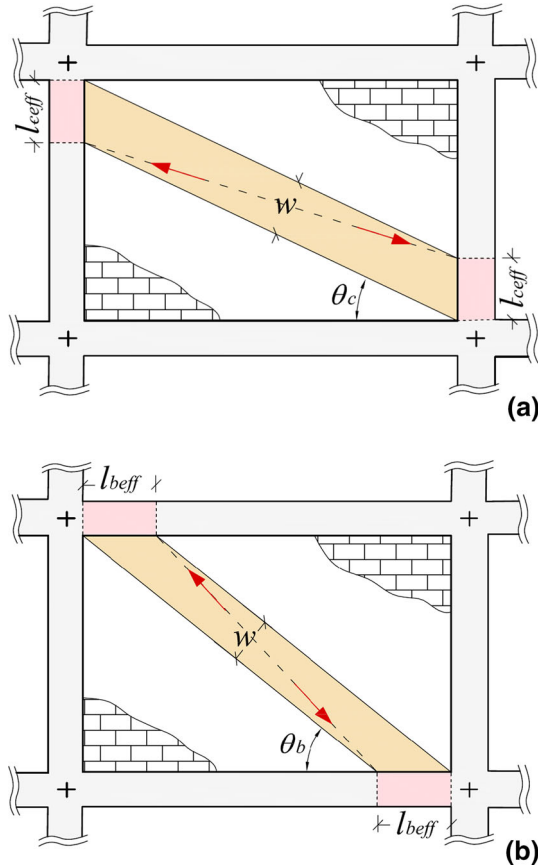
$$l_{beff} = \frac{w}{\sin \theta_b}; \tan \theta_b = \frac{h}{l - l_{beff}} \tag{4}$$

Although the question of local failure of RC members adjacent to infills is treated in FEMA 356 more than in other codes, the strategies suggested, not deriving from a specific analysis and basing on expected values for equivalent strut strength may lead to an unreliable estimation.

Considering all premises above, this paper provides a study in which the relevance of the local shear interaction effects is pointed out, giving the basis for a tool as rigorous as it is simple for the prediction of the real distribution of shear demand in the critical sections of frames when a single equivalent concentric strut is used.

The study, regarding a single infilled frame that can be viewed as a part of a more complex framed structure, is based on the comparison of the results derived from two modelling approaches: one (M1 model) providing the simple single-strut approach; the other one (M2 model) using plane–shell elements to model infills, nonlinear beam elements at the contour and multilinear elastic links (MElink) resisting in compression only at the frame–infill interface. Comparisons are carried out, with variation in mechanical features, geometry, stiffening and strength ratios between frame and infill, in order to determine, for fixed interstorey drifts, the relationship between the axial force evaluated on the equivalent strut and the shear forces (negligible in the M1 model) evaluated in critical sections of beams and columns in the M2

**Fig. 4** Schemes for the evaluation of local effects according to FEMA 356: **a** on columns; **b** on beams



model. The final aim is to permit use of the simple equivalent concentric strut approach for the analysis, this approach being able to provide adequate correction coefficients for local shear forces arising in the beams and in the columns near the joints.

This allows to have a wider consciousness of the mechanics of the frame–infill systems varying the characteristics of infills. Further, here, the independence of the level of shear in the columns and beams from the interstorey drift has been proved, thanks to a major and more detailed numerical simulations, providing a decisive advance for the future of the prediction of local effects in infilled frames. Hence an updated tool for the prediction of the above effects has been presented. Finally a comparison has been made between the tool proposed here and the strategy proposed by FEMA for the prediction of the shear due to infills in frame members.

## 2 Modelling

As mentioned above the results of this work are based on a comparative procedure between two different approaches used to model the same structural system. Having as reference the generic infilled frame, whose geometrical features are indicated in Fig. 5, the structural responses at fixed interstorey drifts are compared in detail. The M1 model (Fig. 6) is based

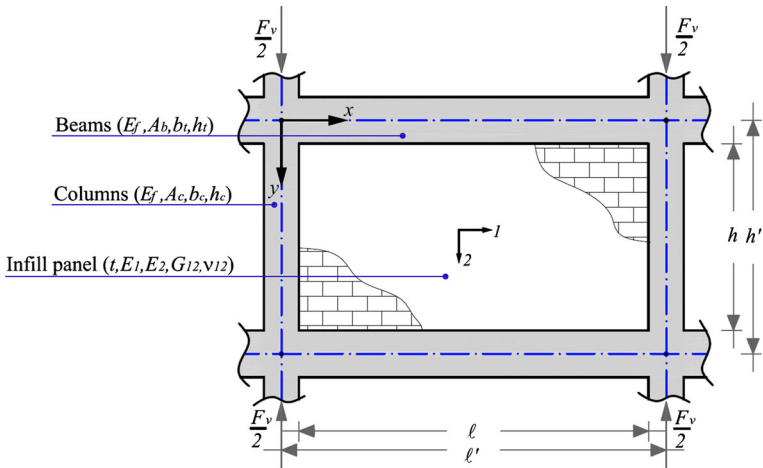
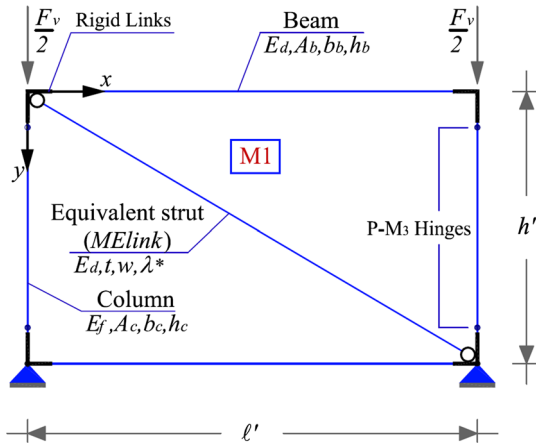


Fig. 5 Generic features of an infilled frame

Fig. 6 M1 model: geometrical and mechanical scheme



on the classical assumption of replacing an infill with an equivalent diagonal concentric strut. This model requires a very low computational effort and is really efficient when nonlinear analyses have to be carried out, although it is affected by a significant defect due to the impossibility of evaluating the interferences of infills in local internal force distribution on the RC members. The M2 model (Fig. 8), which instead requires a higher computational effort, allows one to evaluate the influence of the infill on the internal forces in RC members thanks to the modelling of the infill in finite elements connected to beams and columns through interfaces elements able to transfer normal forces to the surrounding frame.

Models M1 and M2 can be considered equivalent and results can be compared under monotonic loading when they exhibit the same stiffness in both the linear and nonlinear fields. More generally, the stiffness equivalence can be defined as a function of interstorey drift ( $d_r$ ) and expressed by the equation

$$K_{M1}(d_r) = K_{M2}(d_r) \tag{5}$$

$K_{M1}(d_r)$  and  $K_{M2}(d_r)$  being the lateral secant stiffness of the M1 and M2 models for a generically assigned  $d_r$ .

Analyses and modelling were performed using SAP 2000 NL. The characterization of the M1 and M2 models is indicated below, while the details of comparisons procedures and results are discussed in the following sections.

### 2.1 M1 model

The M1 model (Fig. 6) is obtained by the application of the equivalent strut approach. The geometrical and mechanical characteristics of the RC infilled frame from which it is originated are shown in Fig. 5. There,  $b_b$  and  $h_b$  are the width and the depth of the beam cross-sections, respectively and  $A_b$  the corresponding area, while  $b_c$  and  $h_c$  are the width and the depth of the column cross-sections, respectively and  $A_c$  the area. Regarding to the elastic parameters, the concrete constituting the frame is identified by the Young modulus  $E_f$ , while masonry constituting infills is mechanically characterized by the parameters  $E_1$ ,  $E_2$ ,  $G_{12}$ ,  $\nu_{12}$  which are respectively the Young moduli, rigidity modulus and Poisson ratio referred to directions 1 and 2.

The identification of the equivalent diagonal strut cross-section width  $w$  is performed by means of the expression below (Papia et al. 2003).

$$w = d \kappa \frac{c}{z (\lambda^*)^{\beta^*}} \tag{6}$$

where  $d$  is the infill diagonal length and  $c$  and  $\beta^*$  are coefficients depending on the Poisson ratio  $\nu_d$  along the diagonal direction (along which the equivalent strut lies) and are defined by the equations

$$c = 0.249 - 0.0116 \nu_d + 0.567 \nu_d^2 \tag{7}$$

$$\beta^* = 0.146 + 0.0073 \nu_d + 0.126 \nu_d^2, \tag{8}$$

further  $z$  is a coefficient depending on the panel shape and can be evaluated as

$$z = 1 + 0.25(\ell/h - 1) \tag{9}$$

where  $\ell$  and  $h$  are the infill dimensions. The coefficient  $\kappa$  appearing in Eq. 6 takes into account the effect of the vertical loads which generically act on columns and involve infill panels. This coefficient can be obtained as a function of the mean vertical deformation  $\varepsilon_v$  experienced by columns as effect of the compressive load  $F_v$  (Amato et al. 2008), through the equation

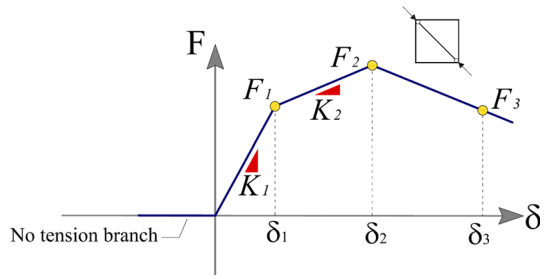
$$\kappa = 1 + (18\lambda^* + 200)\varepsilon_v \tag{10}$$

in which  $\varepsilon_v$  is calculated as

$$\varepsilon_v = \frac{F_v}{2A_c E_f} \tag{11}$$

$E_f$  and  $A_c$  being, as before mentioned, respectively the elastic modulus of the concrete constituting the frame and  $A_c$  of the cross-section areas of the columns ( $A_c$  has to be intended as the average of the column cross-section areas in the case of different columns—the elastic modulus  $E_f$  can implicitly include all the phenomena involving the frame in the first loading stage, comprised the first cracking if the vertical loads are not able to prevent it.). Finally the parameter  $\lambda^*$  (Eqs. 6 and 10), is a parameter representative of the frame–infill system and

**Fig. 7** Axial force–axial displacement law for equivalent diagonal strut



characterizes the stiffness ratios between infill and frame: it is defined as follows:

$$\lambda^* = \frac{E_d t h'}{E_f A_c} \left( \frac{h^2}{\ell'^2} + \frac{1}{4} \frac{A_c \ell'}{A_b h'} \right) \tag{12}$$

where  $E_d$  is the infill elastic modulus along the diagonal direction,  $t$  is the infill thickness,  $h'$  and  $\ell'$  are respectively the frame dimensions in agreement to Fig. 3,  $A_b$  is the average of the cross-section areas of the beams.

The evaluation of masonry elastic Young modulus  $E_d$  and the Poisson ratio  $\nu_d$  along the diagonal direction can be easily carried out as a function of the mechanical parameters mentioned above ( $E_1, E_2, G_{12}, \nu_{12}$ ) according to the procedure proposed in Cavaleri et al. (2014).

The constitutive law that governs the equivalent strut is defined by a trilinear axial force–axial displacement compressive diagram (axial meaning along the direction of the strut) having no tensile strength (Fig. 7) in which the initial elastic stiffness  $K_1$  is evaluated as

$$K_1 = \frac{E_d t w}{d} \tag{13}$$

while the strength at the elastic limit  $F_1$  is defined as a function of the parameter  $\alpha < 1$ , which defines the ratio between the peak strength and the level of the resisting force at the end of the elastic branch, that is

$$F_1 = \alpha F_2 \tag{14}$$

The stiffness in the post-elastic branch  $K_2$  is instead related to the parameter  $\beta$ , which regulates the loss of stiffness after the yielding point with respect to the initial one:

$$K_2 = \beta K_1 \tag{15}$$

The displacements at the elastic limit and peak strength are therefore directly identified as

$$\delta_1 = F_1/K_1; \delta_2 = \delta_1 + (F_2 - F_1)/K_2 \tag{16}$$

The trend of the softening branch is linearized and obtained by connecting points  $F_2 - \delta_2$  and  $F_3 - \delta_3$ , assuming that  $F_3 = 0.7F_2$  and calculating  $\delta_3$  by the expression below (Cavaleri et al. 2005)

$$\delta_3 = \frac{1}{\zeta} \ln \left[ \frac{F_2}{F_3} \exp(\zeta \delta_2) \right] \tag{17}$$

where  $\zeta$  is a coefficient defining the decay velocity of the post peak branch.

The equivalent strut peak strength  $F_2$  is finally determined as a function of the mean shear strength of the masonry infill panel  $f_{v0m}$  as follows:

$$F_2 = f_{v0m} t \ell^* \tag{18}$$



**Table 1** Parameters regulating equivalent diagonal strut constitutive law

$\alpha$	$\beta$	$\zeta$	$f_{v0m}$ (MPa)
0.5	0.15	0.02	0.5–1.07

in which  $\ell^*$  represents the ideal length of the panel that coincides with the real length  $\ell$  in the case of square infills ( $\ell/h = 1$ ) and undergoes a reduction down to  $0.7\ell$  when  $\ell/h = 2$ . This assumption takes into account a strength reduction due to the aspect ratio of the infills, especially for rectangular long infills, experimentally observable (Mehrabi et al. 1996).

The equivalent strut properties are introduced in the model by means of a Multilinear Elastic Link (MELink) element available in the SAP 2000 libraries.

The frame mechanical nonlinearities are introduced by means of 4 interacting axial force-bending moment plastic hinges (P–M) placed at the ends of the columns to be representative of the case of a non-seismically designed strong beam-weak column frame.

The hinge properties depend in each case on the cross-section geometrical features and on the reinforcement.

The concrete strength is assumed to be 25 MPa and an unconfined constitutive law is attributed to consider low transversal reinforcement. The steel rebar strength is set equal to 450 MPa and an elastic perfectly plastic law is attributed. Nodal regions at the intersections between beams and columns are modelled as rigid links. The reinforcement geometrical ratio is set equal to 1% for all column sections and it is furthermore assumed that the beams have a higher flexural strength than the columns, as in the case of structures designed to resist gravity loads only. Finally, a dimensionless axial force  $n = 0.2$  is assigned on top of the columns.

The calibration of the parameters  $\alpha$ ,  $\beta$  and  $\zeta$ , which characterize the shape of the monotonic law of the equivalent strut, were provided by carrying out pushover analyses and comparing them with the experimental results of different types of system tested and available in the literature (e.g. Koutromanos et al. 2011; Cavaleri et al. 2005; Mehrabi et al. 1996; Cavaleri and Di Trapani 2014; Korkmaz et al. 2010; Chiou et al. 1999). Pushover curves were compared with the results of monotonic tests or with the envelope of the strengths of cyclic tests. It has been verified that, meanly, the values for the  $\alpha$ ,  $\beta$  and  $\zeta$  that can be adopted for defining the shape the response of an infilled frame are the ones inserted in Table 1.

Besides, basing on results of experimental tests reported in (Cavaleri et al. 2012, 2014) for different typologies of masonries, it is assumed that the elastic Young modulus ratio  $\gamma = E_1/E_2$  is equal to 0.75, the shear modulus  $G_{12} = 0.4 E_2$  and the Poisson's ratio  $\nu_d = \nu_{12} = 0.1$ . Different values for the shear strength  $f_{v0m}$  of the panels (from 0.50 to 1.07 MPa) are considered in the analyses. The above mentioned parameters governing the equivalent strut compressive law each time are summarized in Table 1.

With regards to the modelling of the frame-strut, when the strategy of substitution of infill with an equivalent strut is adopted, the non exact correspondence between the real state evolution (e.g. cracking pattern, failure modes, etc.) and the model structural state is generally accepted as long as a match, by the global phenomenological point of view, is obtained in lateral stiffness, in lateral strength, in degradation of stiffness and strength, in residual strength, etc. (e.g. Shing and Stavridis 2014; Asteris and Cotsovos 2012; Asteris et al. 2013). This is the natural consequence of the substitution of a substructure (namely an infill) with a deeply different element (namely a strut). The calibration of an equivalent strut able to match the global phenomenon takes account the possibility of formation of plastic hinges at critical regions of frame members. Further, a comparison between the “exact model” and the

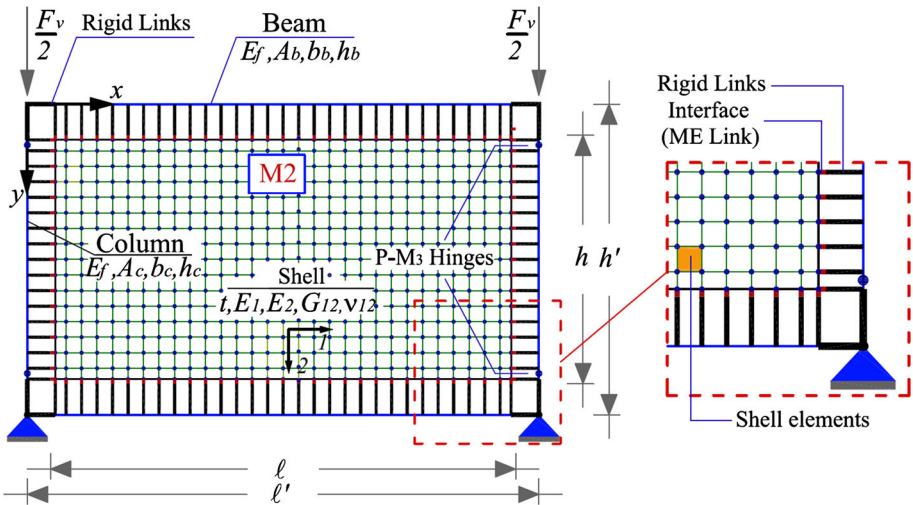


**Fig. 8** M2 model: geometrical and mechanical schemes

simplified model highlights normally a comparable sequence in the formation of the plastic hinges at ends of the columns although this fact cannot be considered a rule (e.g. [Fiore et al. 2012](#))

## 2.2 M2 model

Referring to the generic infilled frame (Fig. 5), the M2 model was also defined (Fig. 8) characterized by detailed discretization of infill by means of orthotropic elastic shell elements. The assumptions for the elastic properties of the masonry (Young moduli  $E_1$  and  $E_2$  along the two orthogonal directions, shear modulus  $G_{12}$  and Poisson ratio  $\nu_{12}$ ) are the same as those proposed for the characterization of the M1 model.

The RC frame at the boundary was modelled as the one included in the M1 model in terms of geometry and properties of concrete and steel rebars. The distance between the infill and the surrounding frame beam elements, which are positioned at the centrelines, is covered by means of null weight rigid links. The latter have the sole function of transmitting the interface forces. A similar approach is also proposed in [Doudoumis \(2007\)](#). Interface elements are placed between shell contour nodes and rigid link ends and are modelled using multilinear elastic link elements having only axial stiffness, no tensile strength and a constitutive law that is assumed to be elastic in compression. As mentioned above the interface elements are used to simulate the mortar joints. Taking into account the high manufacturing variability affecting these mortar joints, the conventional elastic Young modulus  $E_m = 3,000$  MPa was set, and the conventional mortar joint thickness  $h_m = 20$  mm was assigned. Also considering that under lateral loads the frame–infill contact lengths are strongly reduced and mortar joints are affected by significant damage, frictional effects were not included in the model (different studies (e.g. [Asteris 2008](#)) show that friction arising in interfaces is not decisive for the overall response).

It is generally accepted after different numerical tests (e.g. [Fiore et al. 2012](#); [Asteris 2008](#)) that friction does not modify the overall response of an infilled frame.

Nevertheless friction can modify the local response in the sense of a reduction of the stresses normal to the contact surface frame–infill. This produces also a reduction of the

shear stresses on members. The Coulomb law is commonly used for the friction, meaning that the friction stresses can be considered proportional to the stresses normal to the contact frame–infill surface. The using of this approach requests the definition of a proportionality factor (the friction coefficient  $m$ ) but it is not simply to fix a realistic value of it. For example in [Papia et al. \(2003\)](#) and in [Saneinejad and Hobbs \(1995\)](#) the value 0.45 has been assigned for the friction coefficient without an experimental evidence while in [Fiore et al. \(2012\)](#) a parametric study has been preferred and carried out assigning values in the range 0–0.4. Further the friction phenomenon is not simply controllable in the case of cyclic loading: it can undergo a strongly variation with the increasing of the numbers of cycles. In this conditions, considering that (a) it does not influence the overall behaviour of the system, (b) it produces a reduction of the shear stresses on beams and columns, (c) it progressively varies in the case of cyclic loading, it is reasonable to neglect it in the assessment of the local shear effect on frame members.

Nonlinearity of shell elements was introduced in the model by iteratively scaling (i.e. reducing) their thickness. The reduced thickness ideally represents that one allowing to obtain for the M2 model the same lateral secant stiffness as exhibited by the M1 model for a fixed interstorey drift level. This way the simple M1 model permits one to calibrate the M2 model at each selected prescribed displacement basing on a nonlinear law assumed for the equivalent strut.

The so defined M2 model furnishes more detailed results regarding frame internal force modification due to the frame–infill interaction, being able to simulate both interface detachment and local shear effects on RC member ends, unlike the M1 model, able to simulate the overall behaviour but not the distribution of the internal forces in the frame members.

### 2.3 Reliability of M1 and M2 models

Both M1 and M2 models are characterized by non linear frame members whose nonlinearity depends on the possibility of activation of plastic hinges in the critical regions. Considered that the M1 model reproduces infill by an equivalent nonlinear diagonal strut and M2 model reproduces infill by means of linear Finite Shell Elements, the reliability of the M2 nonlinear model is obtained by a calibration basing on the response of the M1 nonlinear model at each assigned drift. On the other hand the M1 nonlinear model is calibrated basing on experimental tests. Therefore M2 model, because of the calibration criterion adopted, reproduces the nonlinear behaviour of infilled frames.

The M2 model is calibrated by equating its secant stiffness and the M1 model secant stiffness at each assigned drift. In this way, as schematically shown in [Fig. 9](#), the M2 model can follow the response of the M1 model. This is possible assuming each time different mechanical parameters. In this case, considering that the nonlinearity of the members is obtained by plastic hinges at the critical regions fixed as a functions of the cross sections characteristics, the equivalence is obtained only by varying the thickness of the infill that is modelled at each stage as a linear material.

The definition of the infill nonlinearities of the refined M2 model, carried out by a comparison with the M1 model, has great advantages. In fact infill is generally a non homogeneous material whose nonlinear behaviour depends on a number of parameters whose identification requests a non negligible effort (e.g. [Stavridis and Shing 2010](#)). Conversely the behaviour of an equivalent nonlinear strut can be defined depending on a minor numbers of parameters more simply identifiable by observing experimental responses.

For what above the reliability of the M2 model depends on the reliability of the M1 model whose characteristics has been discussed in previous Sect. 2.1. M1 model has been

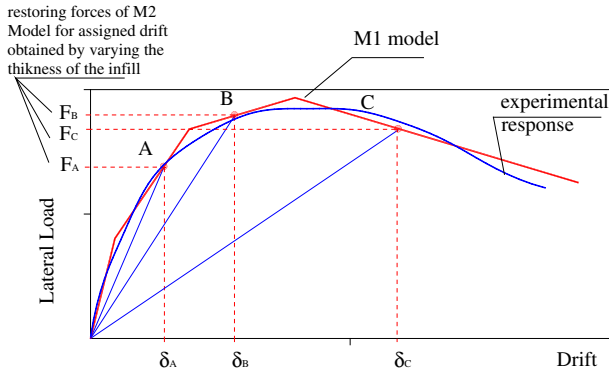


**Fig. 9** Theoretical representation of three states of the M2 model (points A, B, C) in the lateral force–drift curve compared to the response of the M1 model and the experimental response

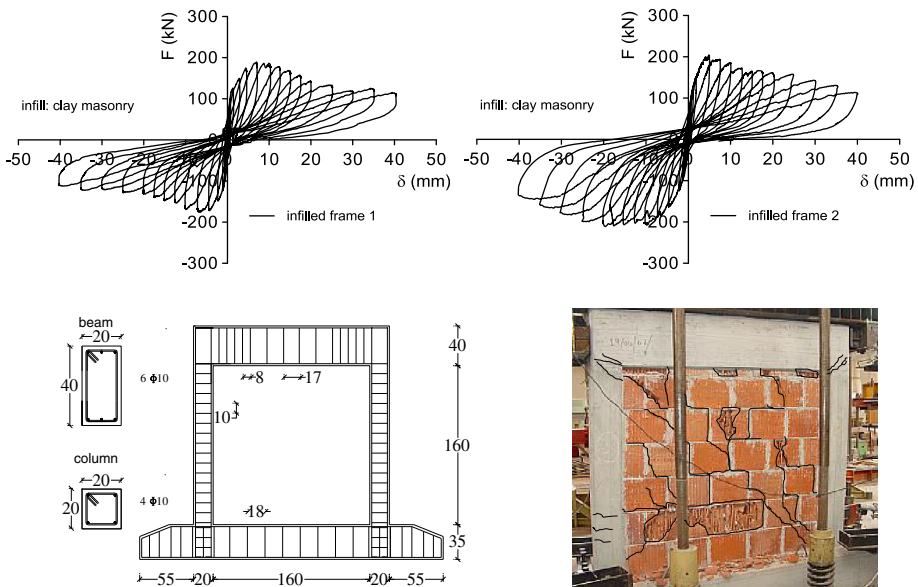


**Fig. 10** Experimental responses of infilled frames (Cavaleri et al. 2014)

formulated on the basis of different experimental results available in the literature. As an example in Fig. 10 the cyclic responses of two frames infilled with clay masonry, obtained by the authors and partially discussed in Cavaleri et al. (2014), used for the calibration of the M1 model, are shown. Also a comparison of the envelopes of strengths with the M1 model is inserted in Fig. 11 proving the reliability of the model M1 itself. To the same conclusions one can arrive by a comparison with the experimental results in Koutroumanos et al. (2011) (see Fig. 12), Korkmaz et al. (2010) and Chiou et al. (1999).

The approach above described uniformly spreads the damage in the infill but this fact does not contrast the reliability of the results in fact the experimental observations in the case of cyclic loading show a wide diffusion of the damage (see Fig. 10) further the damage does not change the influence of the ineffective infill volumes, if any.

**Fig. 11** Experimental strength envelopes of infilled frames compared to analytical one obtained by assigning the strut M1 model (Cavaleri and Di Trapani 2014)

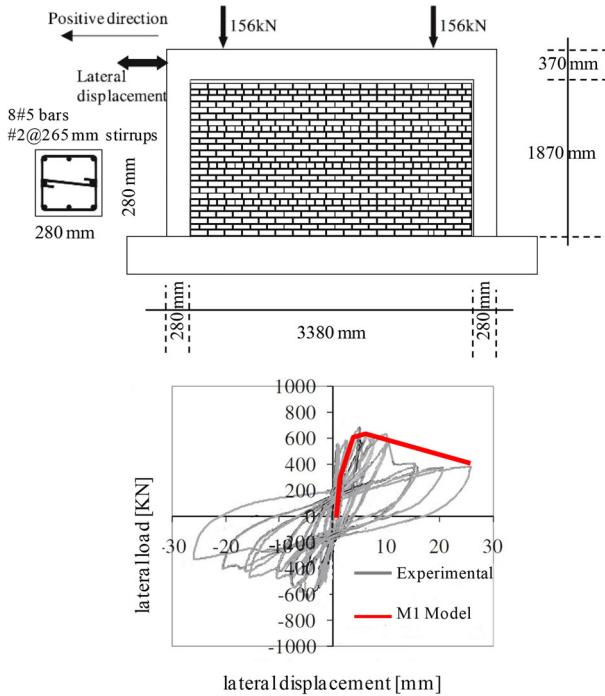
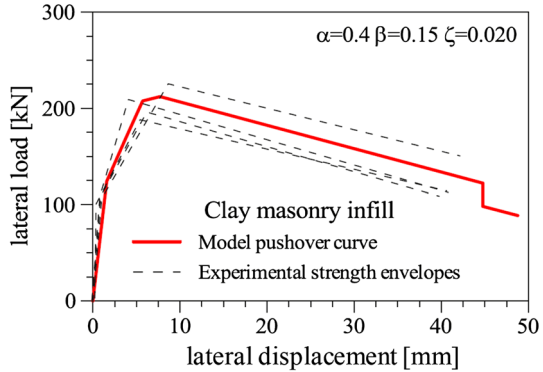
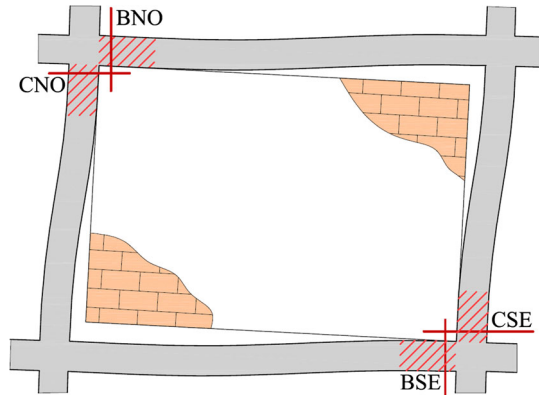


**Fig. 12** Experimental response of an infilled frame (Koutromanos et al. 2011) compared to the analytical envelope obtained by assigning the strut M1 model

### 3 Parametric study

As discussed in the previous section, the comparability of the two-models used here is possible, under monotonic loading, when they exhibit the same stiffness at a generically assigned interstorey drift. Therefore the procedure used to evaluate internal force modification due to the presence of infill panels follows the steps shown above: (a) assignment of the mechanical properties and geometry of the infilled frame; (b) definition of the equivalent strut (M1 model); (c) definition of the M2 model in which the thickness ( $t$ ) of the infill is initially set equal to the real thickness; (d) choice of an interstorey drift ( $d_r$ ); (e) analysis

**Fig. 13** Critical sections on RC frame



of the M1 model by imposing the fixed interstorey drift and evaluation of secant stiffness as the parameter identifying damage level; (f) identification of the damage level in the M2 model (by reducing infill thickness) in such a way as to provide the same secant stiffness as exhibited by the M1 model; (g) evaluation of RC frame internal force distribution on the M2 model. Once the internal force distribution is evaluated for both the M1 and M2 models it is possible to correlate the level of the shear forces acting in the critical sections of the frame members (obtained by the M2 model) and the axial force in the equivalent strut.

Parametric analyses were carried out to evaluate the responses, for an assigned damage level (identified by the interstorey drift ratio), of infilled frames modelled by means of both the approaches described above. The geometrical and mechanical properties of frames and infills (elastic moduli, aspect ratio, beam element cross-sections, masonry mechanical characteristics) were varied in order to evaluate their influence on the distribution of shear forces occurring on beam and column ends in contact with infills.

The shear force in the four critical sections indicated in Fig. 13 (BNO-Beam North-West, BSE-Beam South-East, CNO-Columns North West, CSE-Columns South East) was considered. In these sections, equilibrium with forces transferred by the infill through the contact regions has to be granted, thus the shear demand is here highly concentrated.

For each infilled frame considered, M1 and M2 models were generated and analyzed for the drifts fixed above. Once the structural responses were obtained the dimensionless quantities reported below were evaluated:

$$\alpha_{BNO} = \frac{V_{BNO}^{(M_2)}}{N_p^{(M_1)}}; \quad \alpha_{BSE} = \frac{V_{BSE}^{(M_2)}}{N_p^{(M_1)}} \tag{19}$$

$$\alpha_{CNO} = \frac{V_{CNO}^{(M_2)}}{N_p^{(M_1)}}; \quad \alpha_{CSE} = \frac{V_{CSE}^{(M_2)}}{N_p^{(M_1)}} \tag{20}$$

in which  $N_p^{(M_1)}$  is the axial force on the equivalent diagonal strut evaluated in the M1 model while  $V_{BNO}^{(M_2)}, V_{BSE}^{(M_2)}, V_{CNO}^{(M_2)}, V_{CSE}^{(M_2)}$ , are the shear forces acting in the critical sections evaluated using the M2 model.

The coefficients  $\alpha_{BNO}, \alpha_{BSE}, \alpha_{CNO}, \alpha_{CSE}$ , here called *shear distribution coefficients*, define the relationship existing between the shear forces acting on the frame critical sections and the axial force acting on the equivalent strut for a fixed interstorey drift ratio. If prediction of shear distribution coefficients is possible a priori as a function of the geometrical and

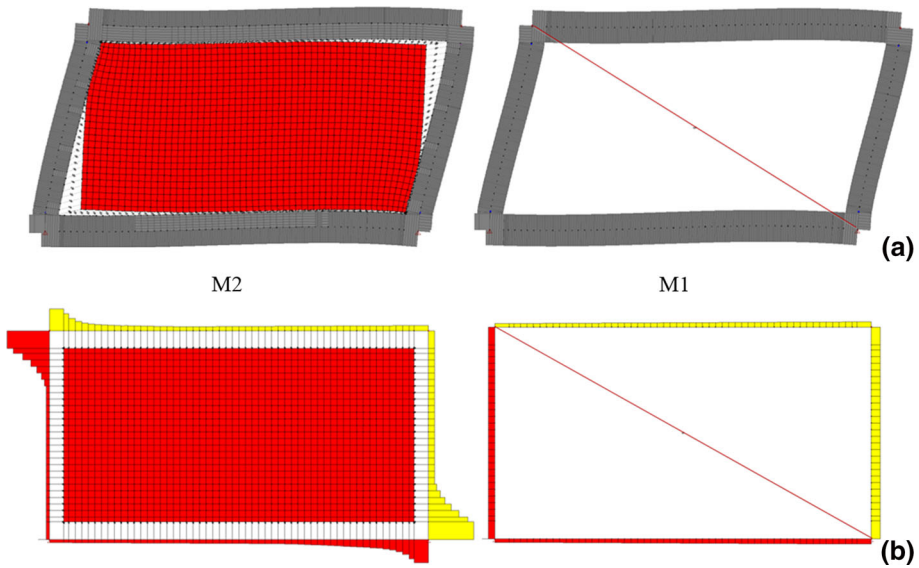


**Fig. 14** Comparison between M1 and M2 model responses: **a** deformed shape; **b** shear distribution

mechanical variables of the infilled frame system, these coefficients become a useful tool to evaluate the real shear forces on frame sections as a quota of the equivalent strut axial force. In Fig. 14, a qualitative comparison in terms of deformed shapes and distribution of shear demand between responses exhibited by the two models for the same interstorey drift is reported, evidencing the relevance of local shear effects detected in the contact regions by the M2 model and not by the M1 model.

Since shear distribution coefficients can be defined at each interstorey drift reached by an infilled frame, a sensitivity analysis for different classes of infilled frames was primarily performed with an increase in the drift level from the elastic phase ( $d_r = 0.01–0.03\%$ ) up to  $d_r = 1.2\%$  which for most non-ductile structural systems represents a near-collapse condition.

It is not easy to identify with a single parameter a class of infilled frame systems because a really wide quantity of variables is involved and the behaviour of each system depends not so much on the single mechanical properties of RC frame and masonry infills but more on their ratios. It is also important to underline that, since the analyses were carried out in a nonlinear field, parameters that usually are not significant in elastic studies, such as strengths and strength ratios, have to be taken into account. Therefore in this study the parameter  $\psi$  (Eq. 21) was considered as characterising the system; this parameter is the product of three terms that appear to be fundamental in the behaviour of an infilled frame.

$$\psi = \lambda^* \xi^* f_{v0m} \tag{21}$$

The parameter  $\lambda^*$  appearing in Eq. 21 has already been defined by Eq. 12. It carries information about the geometry of the system and the stiffness ratio between infill and frame. The term  $\xi^* = M_{RB}/M_{RC}$ , is the ratio between the flexural strengths of the upper beam ( $M_{RB}$ ) and the mean flexural strengths of columns ( $M_{RC}$ ) and is introduced since it is related to the plastic hinge formation sequence that significantly influences frame secant stiffness in the nonlinear field and therefore also the shear distribution coefficient trend. Since the resisting



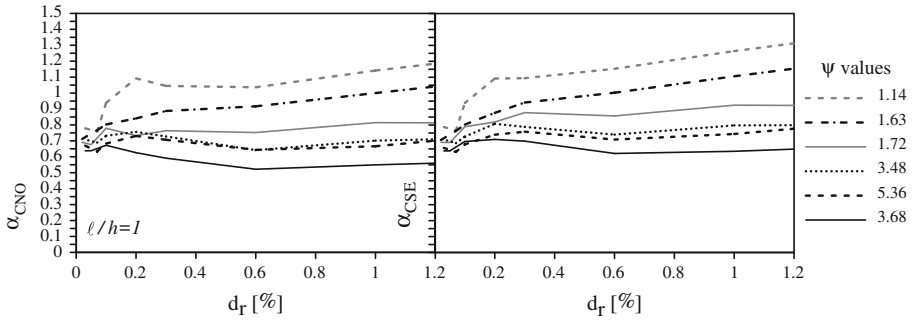


**Fig. 15** Shear distribution coefficients  $\alpha_{CNO}$  and  $\alpha_{CSE}$  versus drift ratio for different  $\psi$  values and  $\ell/h = 1$

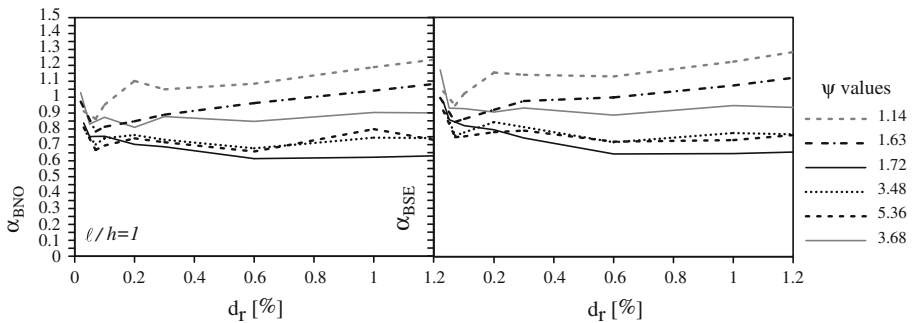


**Fig. 16** Shear distribution coefficients  $\alpha_{BNO}$  and  $\alpha_{BSE}$  versus drift ratio for different  $\psi$  values and  $\ell/h = 1$

moment of the column does not have a univocal value but depends on the axial force, the term  $\xi^*$  can be more simply estimated, as was done in this case, by calculating the ratio  $h_b/h_c$  between the beam and column cross-section heights. Finally,  $f_{v0m}$  is the medium shear strength to be attributed to the masonry used for the infill. This medium shear strength plays a significant role because the forces that are transferred from the infill panel to the RC frame are strongly related to the panel strength.

In Figs. 15, 16, 17 and 18 the results of the previously mentioned sensitivity analyses are shown. In detail the shear distribution coefficients are shown for different values of the  $\psi$  factor and for infilled frames having aspect ratios  $\ell/h = 1$  and  $\ell/h = 2$ . From observation of the curves it appears evident that the shear distribution coefficients maintain a sub-horizontal trend after an unstable stage which is limited to low drift values. This trend occurs for shear distribution coefficients of both the beam and column critical sections and for the two aspect ratios of the infill considered. Another characteristic of the shear distribution coefficients is that they assume the highest values when systems are characterized by low values of the  $\psi$  factor. This trend is explained by the fact that low values of the  $\psi$  factor are generally associated with weak infills combined with RC frames having significant stiffness. These conditions produce a reduction in the axial force  $N_p$  in the equivalent strut appearing in Eqs. 19–21 and the correlated growth of the  $\alpha$  coefficients. In Tables 2 and 3 the characteristics of the specimens modelled for obtaining the curves  $\alpha - d_r$  are included.

Since this study aims to provide the basis for a predictive general instrument able to estimate a reliable shear demand in critical sections a relationship was sought between the shear distribution coefficients and geometrical/mechanical features of the infilled frame summa-



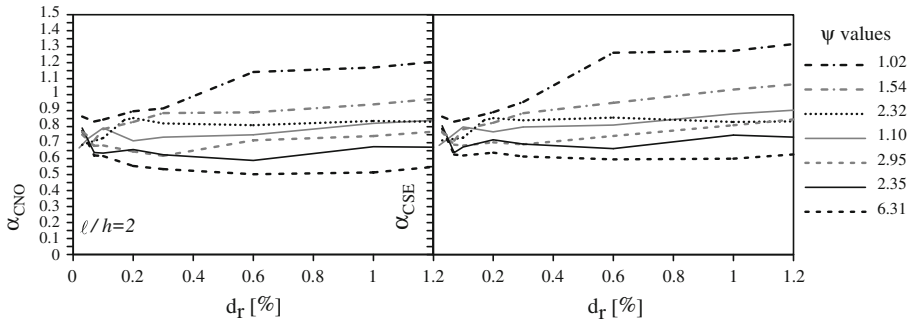


**Fig. 17** Shear distribution coefficients  $\alpha_{CNO}$  and  $\alpha_{CSE}$  versus drift ratio for different  $\psi$  values and  $\ell/h = 2$

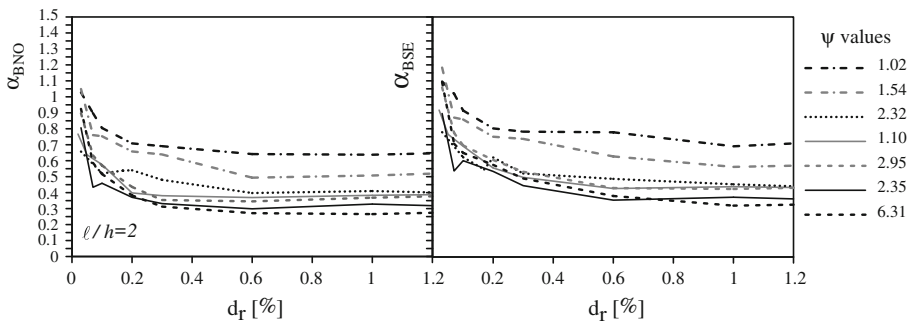


**Fig. 18** Shear distribution coefficients  $\alpha_{BNO}$  and  $\alpha_{BSE}$  versus drift ratio for different  $\psi$  values and  $\ell/h = 2$

rized by the  $\psi$  factor. A further parametric analysis correlating  $\alpha$  coefficients with  $\psi$  factors was therefore performed.

As previously observed, the  $\alpha$  coefficients are almost drift independent after a certain drift level (typically a low value) is reached. Hence it is possible to choose a single interstorey drift value whose corresponding  $\alpha$  coefficients can be considered representative of the frame–infill interaction for each value of the interstorey drift. In order to obtain the previously mentioned  $\alpha - \psi$  correlation, the intermediate drift value  $d_r = 0.6\%$  was selected as a reference. Two sets of models having different infill aspect ratios ( $\ell/h = 1.0$  and  $\ell/h = 2.0$ ) were analyzed. In different cases the above models were characterized by the same or similar values of the parameter  $\psi$  in order to verify that similar values of this parameter produce similar effects in terms of coefficients  $\alpha_{BNO}$ ,  $\alpha_{BSE}$ ,  $\alpha_{CNO}$ ,  $\alpha_{CSE}$ . The results of the analyses in terms of relationships between the  $\psi$  factor and the coefficients  $\alpha_{BNO}$ ,  $\alpha_{BSE}$ ,  $\alpha_{CNO}$ ,  $\alpha_{CSE}$  are synthetically reported in Figs. 19 and 20. The points in Figs. 19 and 20 refer to some of the infilled frames analyzed—in different cases characterized by the same value of  $\psi$  just as a prove that similar values of  $\psi$  generate similar values of the coefficients  $\alpha_{BNO}$ ,  $\alpha_{BSE}$ ,  $\alpha_{CNO}$ ,  $\alpha_{CSE}$ . The points represented in Figs. 19 and 20 refer to infilled frames whose geometrical and mechanical features are indicated in Tables 4 and 5 together with the terms  $\lambda^*$ ,  $\psi$  and  $w$ .

Analytical best fitting functions (Eqs. 22–25) have also been provided in order to show the possibility of deriving effective tools for practical applications. The determination coefficients  $R^2$  are also calculated to evaluate the agreement of the best fitting correlation law with the numerical results.

**Table 2** Characteristics of the specimens producing the results in Figs. 15 and 16

#	$b_c$ (mm)	$h_c$ (mm)	$b_t$ (mm)	$h_t$ (mm)	$h$ (mm)	$\ell$ (mm)	$E_f$ (MPa)	$w$ (mm)	$f_{v0m}$ (MPa)	$\lambda^*$	$\xi^* = M_{RB}/M_{RC}$	$\psi = w\xi^*\lambda^*$
#1	200	200	200	400	1,600	1,600	25,000	623	1.07	1.72	2.00	3.68
#2	200	200	200	400	1,600	1,600	25,000	623	0.50	1.72	2.00	1.72
#3	250	400	250	500	2,700	2,700	25,000	1,034	1.07	2.60	1.25	3.48
#4	250	400	250	500	2,700	2,700	25,000	1,190	1.07	0.85	1.25	1.14
#5	600	300	300	500	2,700	2,700	15,000	1,012	1.07	3.00	1.67	5.35
#6	250	400	250	500	2,700	2,700	25,000	1,034	0.50	2.60	1.25	1.63

**Table 3** Characteristics of the specimens producing the results in Figs. 17 and 18

#	$b_c$ (mm)	$h_c$ (mm)	$b_b$ (mm)	$h_b$ (mm)	$h$ (mm)	$\ell$ (mm)	$E_f$ (MPa)	$w$ (mm)	$f_{i0m}$ (MPa)	$\lambda^*$	$\xi^* = M_{RB}/M_{RC}$	$\psi = w\xi^*\lambda^*$
#1	200	200	200	400	1,600	3,200	25,000	757	1.07	1.10	2.00	2.35
#2	200	200	200	400	1,600	3,200	25,000	757	0.50	1.10	2.00	1.10
#3	250	400	250	500	2,700	5,400	15,000	1,344	1.07	1.73	1.25	2.31
#4	200	200	200	500	1,600	3,200	15,000	748	1.07	2.36	2.50	6.31
#5	200	200	200	500	1,600	3,200	15,000	748	0.50	2.36	2.50	2.95
#6	200	300	200	400	1,600	3,200	15,000	774	0.50	1.54	1.33	1.03
#7	200	300	200	400	1,600	3,200	15,000	774	0.75	1.54	1.33	1.54

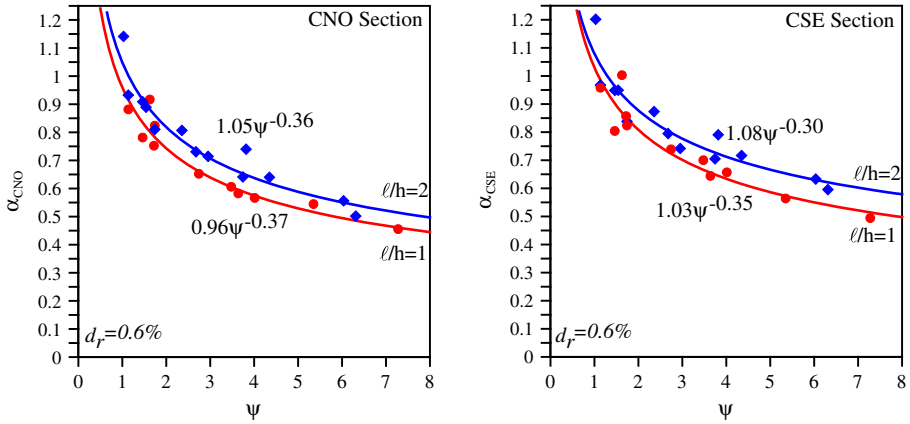


**Fig. 19** Shear distribution coefficients  $\alpha_{CNO}$  and  $\alpha_{CSE}$  versus  $\psi$  factor at  $l/h = 1$  and  $l/h = 2$ . Numerical analysis results and interpolating functions

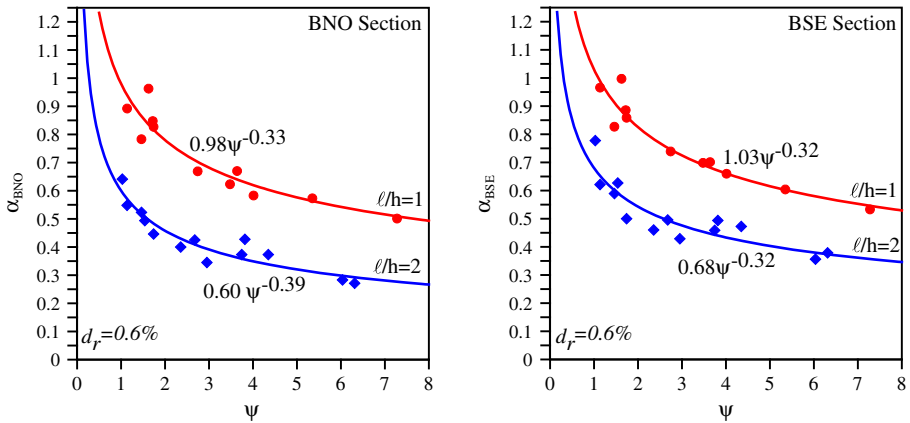


**Fig. 20** Shear distribution coefficients  $\alpha_{BNO}$  and  $\alpha_{BSE}$  versus  $\psi$  factor at  $l/h = 1$  and  $l/h = 2$ . Numerical analysis results and interpolating functions

The laws for the  $\alpha - \psi$  relationships are shown below (including  $R^2$  coefficients) for  $l/h = 1$  (Eqs. 22–23) and for  $l/h = 2$  (Eqs. 24–25)

$$\alpha_{CNO} = 0.96 \psi^{-0.37} (R^2 = 0.94); \quad \alpha_{CSE} = 1.03 \psi^{-0.35} (R^2 = 0.91) \quad (22)$$

$$\alpha_{BNO} = 0.98 \psi^{-0.33} (R^2 = 0.90); \quad \alpha_{BSE} = 1.03 \psi^{-0.32} (R^2 = 0.93) \quad (23)$$

$$\alpha_{CNO} = 1.05 \psi^{-0.36} (R^2 = 0.93); \quad \alpha_{CSE} = 1.08 \psi^{-0.30} (R^2 = 0.90) \quad (24)$$

$$\alpha_{BNO} = 0.60 \psi^{-0.39} (R^2 = 0.88); \quad \alpha_{BSE} = 0.68 \psi^{-0.32} (R^2 = 0.82) \quad (25)$$

By means of the proposed laws  $\alpha$  coefficients can be evaluated for each infilled frame system before analyses are made as a function of the  $\psi$  factor. The above coefficients can be used to correct shear forces detected in critical sections when equivalent strut models are used to perform analyses. Finally, according to Eqs. 19–20 the shear value in critical sections can be evaluated by multiplying the previously calculated  $\alpha$  coefficients by the axial force resulting in the equivalent strut.

By observing the  $\alpha - \psi$  curves it appears evident, as observed before, that, for both aspect ratios considered, the  $\alpha$  coefficients undergo a reduction when the  $\psi$  values increase. This expresses the general tendency of RC frames to receive shear forces on critical sections that increase as the stiffness of the frame increases with respect to the infill. The results also show that the influence of the infill aspect ratio ( $\ell/h$ ) has a major role, especially for beams that are affected by significantly lower shear when the horizontal dimension of the panel  $\ell$  prevails over the height  $h$ .

The results of the analyses reported above can be a basis for assessment of the capacity of RC members of infilled frames when linear or nonlinear analyses are performed by means of equivalent concentric strut models. In practical applications, once the analysis is performed and the axial forces acting on the equivalent struts are known, the shear demand to consider for capacity assessment can be estimated by replacing shear forces on critical sections with the values  $V_{BNO}$ ,  $V_{BSE}$ ,  $V_{CNO}$ ,  $V_{CSE}$  that can be calculated by means of the following expressions:

$$V_{BNO} = V_0 + \alpha_{BNO}N_p; \quad V_{BSE} = V_0 + \alpha_{BSE}N_p \quad (26)$$

$$V_{CNO} = \alpha_{CNO}N_p; \quad V_{CSE} = \alpha_{CSE}N_p \quad (27)$$

$V_0$  being the shear force due to the vertical loads on the beams and  $N_p$  the axial force in the equivalent strut.

#### 4 Extensibility of the laws expressed by Eqs. 22–25

Considering that the laws in question, correlating the coefficients for the right estimation of the shear in the frame members, were obtained for a drift of 0.6%, it is natural to want to verify the extensibility of these laws to different drifts that can be experienced by frame–infill systems.

In this section an application is proposed to two cases of infilled frame having aspect ratios  $\ell/h = 1$  and  $\ell/h = 2$  respectively.

The response in terms of shear demand in the critical section is evaluated for different drift levels using the M2 model and is assumed to be *exact*. The shear distribution is calculated by means of the M1 model and corrected by using the laws in Eqs. 22–25, also for drifts different from 0.6% (lower and higher). Finally, the exact demand (M2 model) and the demand corrected by the proposed law (M1 model) are compared. For the sake of simplicity the term  $V_0$  related to vertical loads is considered null in this example. The geometrical and mechanical characteristics of the models are reported in Table 6 within the  $\psi$  factors and the related shear distribution coefficients calculated by Eqs. 22–25.

The results of the tests are shown in Figs. 21 and 22 in terms of shear on critical sections versus interstorey drifts.

It appears evident that although the proposed strategy is based on shear distribution coefficients evaluated at  $d_r = 0.6\%$ , the resulting predictive capacity at each drift is quite reliable. Prediction errors for the drift levels considered are in most cases acceptable. Figures 21 and 22 also show the level of shear obtainable by the procedure proposed by FEMA. It can be observed that this level of shear agrees conservatively with the maximum level of shear obtainable varying the drift. This result validates the procedure proposed by FEMA but confirms that the shear demand in the frame members may be lower, resulting in a lower effort in the measures to be implemented to obtain a fixed safety level.

**Table 4** Characteristics of the specimens producing the results included in Figs. 19 and 20— $\ell/h = 1$

Spec.	$b_c$ (mm)	$h_c$ (mm)	$b_b$ (mm)	$h_b$ (mm)	$h$ (mm)	$\ell$ (mm)	$E_f$ (MPa)	$w$ (mm)	$f_{i0m}$ (MPa)	$\lambda^*$	$\xi^* = M_{RB}/M_{RC}$	$\psi = w\xi^*\lambda^*$
C1A	200	200	200	400	1,600	1,600	25,000	623	1.07	1.72	2.00	3.68
C2A	200	200	200	400	1,600	1,600	25,000	565	1.07	3.40	2.00	7.28
C3A	250	400	250	500	2,700	2,700	25,000	1,190	1.07	0.85	1.25	1.14
C4A	250	400	250	500	2,700	2,700	25,000	1,190	1.07	1.30	1.25	1.74
C5A	250	400	250	500	2,700	2,700	25,000	1,034	1.07	2.60	1.25	3.48
C6A	250	400	250	500	2,700	2,700	25,000	1,012	1.07	3.00	1.25	4.01
C7A	250	400	250	500	2,700	2,700	25,000	1,067	1.07	2.05	1.25	2.74
C8A	600	300	300	500	2,700	2,700	25,000	1,192	1.07	0.82	1.67	1.46
C9A	600	300	300	500	2,700	2,700	15,000	1,054	1.07	3.00	1.67	5.35
C10A	200	200	200	400	1,600	1,600	25,000	623	0.50	1.72	2.00	1.72
C11A	250	400	250	500	2,700	2,700	25,000	1,034	0.50	2.60	1.25	1.63

**Table 5** Characteristics of the specimens producing the results included in Figs. 19 and 20— $\ell/h = 2$

Spec.	$b_c$ (mm)	$h_c$ (mm)	$b_b$ (mm)	$h_b$ (mm)	$h$ (mm)	$\ell$ (mm)	$E_f$ (MPa)	$w$ (mm)	$f_{i0m}$ (MPa)	$\lambda^*$	$\xi^* = M_{RB}/M_{RC}$	$\psi = w\xi^*\lambda^*$
C1B	200	200	200	400	1,600	3,200	25,000	757	1.07	1.10	2.00	2.35
C2B	200	200	200	400	1,600	3,200	20,000	707	1.07	2.82	2.00	6.03
C3B	200	400	200	500	2,700	5,400	20,000	1,362	1.07	1.30	1.25	1.74
C4B	200	400	200	500	2,700	5,400	20,000	1,368	1.07	2.00	1.25	2.68
C5B	200	400	200	500	2,700	5,400	20,000	1,121	1.07	2.80	1.25	3.75
C6B	200	400	200	500	2,700	5,400	20,000	1,450	1.07	0.85	1.25	1.14
C7B	200	400	200	500	2,700	5,400	20,000	1,200	1.07	3.25	1.25	4.35
C8B	600	300	300	500	2,700	5,400	20,000	1,453	1.07	0.82	1.67	1.46
C9B	600	300	300	500	2,700	5,400	20,000	1,293	1.07	2.14	1.67	3.82
C10B	200	200	200	500	1,600	3,200	15,000	748	1.07	2.36	2.50	6.31
C11B	200	200	200	500	1,600	3,200	15,000	748	0.50	2.36	2.50	2.95
C12B	200	300	200	400	1,600	3,200	15,000	774	0.50	1.54	1.33	1.03
C13B	200	300	200	400	1,600	3,200	15,000	774	0.75	1.54	1.33	1.54

**Table 6** Geometrical and mechanical characteristics of models used for validation tests

#	$\ell/h$	$b_c$ (mm)	$h_c$ (mm)	$b_b$ (mm)	$h_b$ (mm)	$h$ (mm)	$\ell$ (mm)	$Ef$ (MPa)	$w$ (mm)	$f_{i0m}$ (MPa)	$\lambda^*$	$\xi^* = MRB/MRC$	$\psi = w\xi^*\lambda^*$	$\alpha_{CNO}$	$\alpha_{CSE}$	$\alpha_{BNO}$	$\alpha_{BSE}$
#1	1.0	250	400	250	500	2,700	2,700	25,000	1,034	1.07	2.60	1.25	3.48	0.605	0.666	0.649	0.691
#2	2.0	200	300	200	400	1,600	3,200	15,000	774	0.50	1.54	1.33	1.02	1.043	1.074	0.595	0.676



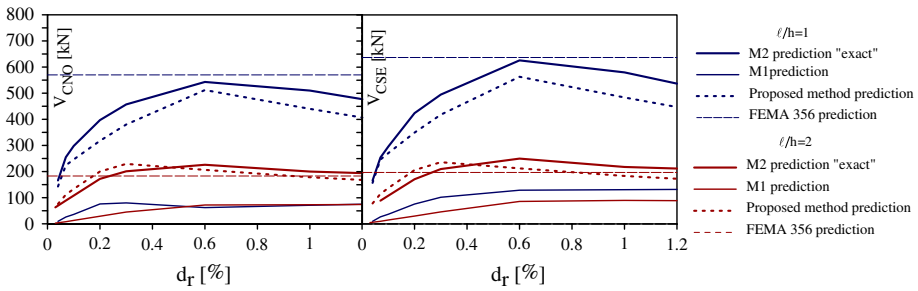


**Fig. 21** Comparison of the predictive capacity of shear forces on column critical sections in the M1 Model and proposed method with respect to the M2 Model for two numerical specimens characterized by  $l/h = 1$  and  $l/h = 2$

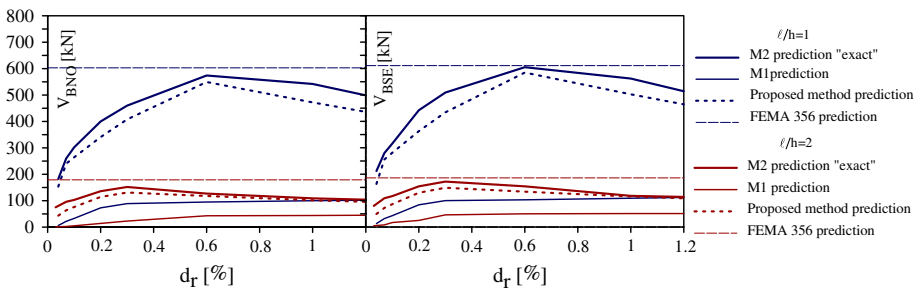


**Fig. 22** Comparison of the predictive capacity of shear forces on beam critical sections in the M1 Model and proposed method with respect to the M2 Model for two numerical specimens characterized by  $l/h = 1$  and  $l/h = 2$

### 5 Conclusions

In the present paper a study of the local shear effects produced at the ends of beams and columns of non-ductile RC infilled frames in the presence of lateral loads has been presented. This study has the aim of providing strategies for correcting the results in terms of shear demand obtained when, for the modelling, an infill is substituted with an equivalent concentric strut.

A comparison has been carried out between the force arising in the frame members in the case of an infill modelled as an equivalent concentric strut and in the case of an infill “exactly” modelled by finite shell elements, at different drift levels, for a single infilled frame. The comparison was repeated varying the geometrical and mechanical characteristics of the frame–infill system and a correlation law between a parameter synthesizing the characteristics of frame and infill and the real shear distribution in the critical sections was derived. This law allows one to express the local shear forces acting on beam and column ends as a fraction of the axial load experienced by the equivalent strut and for this reason it can be considered a basis for a predictive tool to be used for the assessment of shear demand on RC member critical sections that is otherwise undetectable when a simple equivalent concentric strut model is used. The predictive capacity of the correlation proposed was tested on two numerical specimens having two different aspect ratios, demonstrating good accuracy for all investigated drifts. Further, a comparison was made with the shear demand assessment proposed by FEMA, confirming on one hand the reliability of the approach proposed (a light

underestimation of the model proposed in FEMA for the shear demand in the columns in the case of rectangular infills is not really significant) and on the other one the possibility of an overestimation of the FEMA approach for drifts lower than those for which the equivalent strut is affected by a force equal to its resistance.

The proposed correlation is obtained considering mechanical properties and structure configurations representative of RC frames designed to resist vertical loads only, but the study can be improved by including a wider class of infilled frames. However, it reveals that more accurate assessment of local shear effects is achievable even if detailed and onerous models are not used to perform analyses. Further, instruments supplementing technical codes which do not provide any predictive strategy for the evaluation of local frame–infill interaction effects or give very conservative approaches can be formulated.

**Acknowledgments** This study was sponsored by ReLUIS, Rete di Laboratori Universitari di Ingegneria Sismica, Linea 2, Obiettivo 5: Influenza della Tamponatura sulla Risposta Strutturale.

## 6 Appendix: Reliability of the internal forces transferred from infill to frame members as predicted by M2 simplified FE model

According to the procedure described in Sect. 2.2, when using M2 model, the nonlinearity of infills (modelled by shells), is introduced by a multi-stage linear equivalence. The latter is obtained scaling the thickness of the infill in such a way to get the same secant stiffness of M1 model at each interstorey drift. In terms of global behaviour the procedure provides the same level accuracy of the one provided by M1 model. This means that if M1 model is well calibrated the overall response obtained by M2 is accurate too. The accuracy of M2 model in prediction of local response in terms of shear action transferred to frame members is a question to discuss but not simply to definitively solve: really if one has to fix as “true” the response of a more refined model including the nonlinearity of infills it has to be said that there are so many approaches in defining the nonlinearity of a shell system hence the choice of a “true” model is itself a problem.

Anyway, for the case here discussed, a comparison between the M2 multistage linear equivalent model, used through the paper to estimate the internal forces on the frame members, and a fully nonlinear version of the M2 model before mentioned (having the characteristics specified below) has been carried out. The results obtainable by the two models have been compared in terms of global response (base shear vs. interstorey drift) and local response

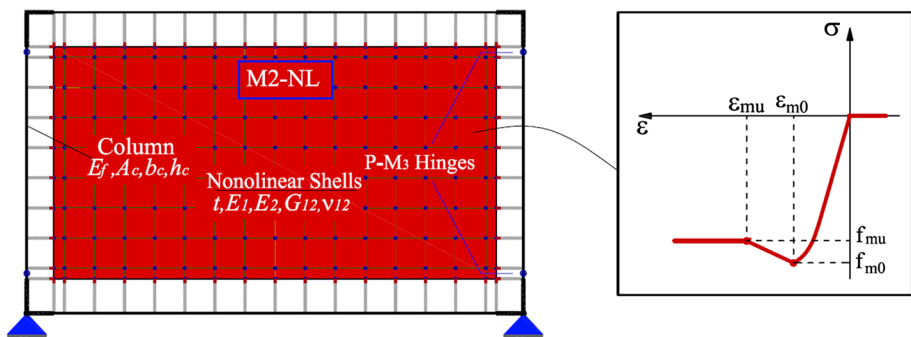


**Fig. 23** M2 model with nonlinear shells

**Table 7** Geometrical and mechanical characteristics of the specimen used for the comparison

Spec.	$b_c$ (mm)	$h_c$ (mm)	$b_b$ (mm)	$h_b$ (mm)	$h$ (mm)	$\ell$ (mm)	$E_f$ (MPa)	$E_1$ (MPa)	$E_2$ (MPa)	$G_{12}$ (MPa)	$\nu_{12}$ (MPa)	$w$ (mm)	$f_{v0m}$ (mm)	$\lambda^*$	$\xi^*$	$\psi$
S1B (Cavaleri and Di Trapani 2014)	200	200	200	400	1,600	1,600	25,000	5,038	6,401	2,574	0.07	623	1.07	1.72	2.00	3.68

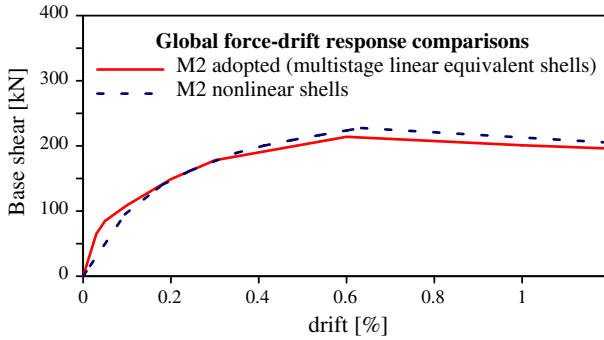


**Fig. 24** Comparison between the global force–drift responses obtained by a M2 fully nonlinear model and the M2 multistage linear model used through the paper

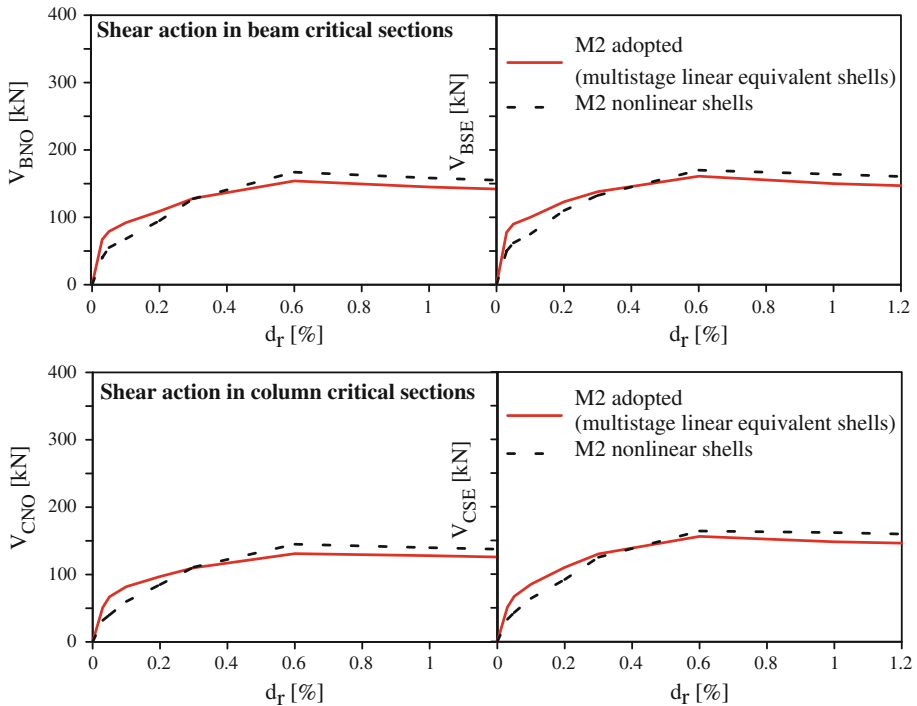


**Fig. 25** Comparison between the local shear force–drift responses obtained by a M2 fully nonlinear model and the M2 multistage linear model used through the paper

(shear in critical section vs. interstorey drift). The refined fully nonlinear M2 model included orthotropic nonlinear shell elements (Fig. 23). The nonlinear behaviour of the shells was attributed after an equivalent homogenization of the masonry material using the compressive stress–strain law (parabolic-linear-constant) reported in Fig. 23. The characteristic strains  $\varepsilon_{m0}$  and  $\varepsilon_{mu}$  were fixed at the values 0.002 and 0.0035, respectively. A peak strength  $f_{m0} = 8.66$  MPa was assumed, having as reference the experimental results reported in Cavaleri and Di Trapani (2014) for clay masonry infills. The ratio between ultimate strength  $f_{mu}$  and peak

strength  $f_{m0}$  was assumed to be 0.85. All the other geometrical and mechanical features of the infilled frame are still referred to S1B specimens investigated in Cavaleri and Di Trapani (2014) and reported in Table 7.

As before mentioned the first comparison between the two approaches is made in terms of global force–displacement response. A pushover curve of the M2 nonlinear shell model is compared with the response obtained by the application of the multistage linear procedure. The results are shown in Fig. 24. The curves show that the multistage procedure has a good accuracy in estimating the overall response with a slight overestimation in correspondence of the lower drifts. This trend is reflected on the local shear–drift curves determined for critical sections CNO, CSE, BNO, BSE (Fig. 25). Here the comparison with the fully nonlinear model shows that the prediction of internal shear forces performed by M2 linear equivalent procedure provides a realistic overview. The lower accuracy in earlier drift does not modify the overall reliability since the higher shear actions transmitted by the infills to the frames are associated with larger drifts (where the predictive capability of the procedure is more accurate).

Similar results can be found changing the characteristics of the infilled frame proving that the approach used through the paper considering the non linearity of infills by a multistage linearization procedure, in connections with the objectives fixed, is a valid alternative to more refined models including infill nonlinearity.

## References

- Amato G, Fossetti M, Cavaleri L, Papia M (2008) An updated model of equivalent diagonal strut for infill panels. In: Proceedings of Eurocode 8 perspectives from Italian standpoint, workshop. Napoli, Italy
- Asteris PG (2003) Lateral stiffness of brick masonry infilled plane frames. *J Struct Eng ASCE* 129(8):1071–1079
- Asteris PG (2008) Finite element micro-modeling of infilled frames. *Electron J Struct Eng* 8:1–11
- Asteris PG, Antoniou ST, Sophianopoulos DS, Chrysostomou CZ (2011) Mathematical macromodeling of infilled frames: state of the art. *J Struct Eng ASCE* 137(12):1508–1517
- Asteris PG, Cotsovos DM (2012) Numerical investigation of the effect of infill walls on the structural response of RC frames. *Open Constr Build Technol J* 6(1):164–181
- Asteris PG, Cotsovos DM, Chrysostomou CZ, Mohebkah A, Al-Chaar GK (2013) Mathematical micromodeling of infilled frames: state of the art. *Eng Struct* 56:1905–1921
- Cavaleri L, Di Trapani F (2014) Cyclic response of masonry infilled RC frames: experimental results and simplified modeling. *Soil Dyn Earthq Eng* 65:224–242. doi:10.1016/j.soildyn.2014.06.016
- Cavaleri L, Di Trapani F, Macaluso G, Papia M (2012) Reliability of code proposed models for assessment of masonry elastic moduli. *Ing Sismica* 29(1):38–59
- Cavaleri L, Di Trapani F, Macaluso G, Papia M, Colajanni P (2014) Definition of diagonal Poisson's ratio and elastic modulus for infill masonry walls. *Mater Struct* 47:239–262
- Cavaleri L, Fossetti M, Papia M (2005) Infilled frames: developments in the evaluation of cyclic behavior under lateral loads. *Struct Eng Mech* 21(4):469–494
- Cavaleri L, Papia M (2003) A new dynamic identification technique: application to the evaluation of the equivalent strut for infilled frames. *Eng Struct* 25:889–901
- Chiou YJ, Tzeng JC, Liou YW (1999) Experimental and analytical study of masonry infilled frames. *J Struct Eng ASCE* 125(10):1109–1117
- Chrysostomou CZ, Asteris PG (2012) On the in-plane properties and capacities of infilled frames. *Eng Struct* 41:385–402
- Crisafulli FJ, Carr AJ (2007) Proposed macro-model for the analysis of infilled frame structures. *Bull N Z Soc Earth Eng* 40(2):69–77
- Crisafulli FJ, Carr AJ, Park R (2000) Analytical modelling of infilled frames structures: a general review. *Bull N Z Soc Earth Eng* 33(1):30–47
- D.M. LL. PP. 14 Gennaio 2008. Nuove norme tecniche per le costruzioni
- Doudoumis IN (2007) Finite element modelling and investigation of the behaviour of elastic infilled frames under monotonic loading. *Eng Struct* 29(6):1004–1024

- Eurocode 8 Design of structures for earthquake resistance—Part 1: General rules, seismic actions and rules for buildings. European Committee for Standardization, Brussels
- FEMA 356 (2000) Prestandard and commentary for the seismic rehabilitation of buildings. Federal Emergency Management Agency, Washington
- Fiore A, Netti A, Monaco P (2012) The influence of masonry infill on the seismic behavior of RC frame buildings. *Eng Struct* 44:133–145
- Ghosh AK, Made AM (2002) Finite element analysis of infilled frames. *J Struct Eng ASCE* 128(7):881–889
- Holmes M (1961) Steel frames with brickwork and concrete infilling. In: *Proceedings of Institute of Civil Engineering*, Paper No. 6501, pp 473–478
- Korkmaz SZ, Kamanli M, Korkmaz HH, Donduren MS, Cogurcu MT (2010) Experimental study on the behaviour of nonductile infilled RC frames strengthened with external mesh reinforcement and plaster composite. *Nat Hazards Earth Syst Sci* 10:2305–2316
- Koutromanos I, Stavridis A, Shing PB, Willam K (2011) Numerical modeling of masonry-infilled RC frames subjected to seismic loads. *Comput Struct* 89(11–12):1026–1037
- Mallick DV, Severn RT (1967) The behaviour of infilled frames under static loading. *Proc Inst Civ Eng* 38:639–656
- Mehrabi AB, Shing PB (1997) Finite element modelling of masonry-infilled RC frames. *J Struct Eng ASCE* 123(5):604–613
- Mehrabi AB, Shing PB, Schuller MP, Noland JL (1996) Experimental Evaluation of Masonry-Infilled RC Frames. *J Struct Eng ASCE* 122(3):228–237
- Papia M, Cavaleri L, Fossetti M (2003) Infilled frames: developments in the evaluation of the stiffening effect of infills. *Struct Eng Mech* 16(6):675–693
- Saneinejad A, Hobbs B (1995) Inelastic design of infilled frames. *J Struct Eng ASCE* 121(4):634–650
- Shing PB, Mehrabi AB (2002) Behaviour and analysis of masonry-infilled frames. *Prog Struct Eng Mater* 4(3):320–331
- Shing PB, Stavridis A (2014) Analysis of seismic response of masonry-infilled RC frames through collapse. *ACI Struct J Spec Pap* 297:1–20
- Stavridis A, Shing PB (2010) Finite-element modeling of nonlinear behavior of masonry-infilled RC frames. *J Struct Eng ASCE* 136(3):285–296